Physica E 54 (2013) 53–58

Contents lists available at SciVerse ScienceDirect

Physica E

journal homepage: www.elsevier.com/locate/physe

ZnO nanotubes: Controllable synthesis and tunable UV emission modulated by the wall thickness

Lili Yang [a,b,c], Zhiqiang Zhang [a,c], Zhe Wang [a,c], Yunfei Sun [d], Ming Gao [a,c,d], Jinghai Yang [a,c,*], Yongsheng Yan [b]

[a] Institute of Condensed State Physics, Jilin Normal University, Siping 136000, China
[b] Institute of Chemistry and Chemical Engineering, Jiangsu University, Zhenjiang 212013, China
[c] Key Laboratory of Functional Materials Physics and Chemistry (Jilin Normal University), Ministry of Education, Siping 136000, China
[d] Key Laboratory of Excited State Physics, Changchun Institute of Optics Fine Mechanics and Physics, Chinese Academy of Sciences, Changchun, 130033, China

HIGHLIGHTS

- We report the spin-polarized transport in a system based fully on graphene.
- Our system consists of a zigzag edge nanoflake connected to two nanoribbons as electrodes.
- We consider the effect of impurity in this system in three different configurations.
- We demonstrate that the pure system shows high spin filtering properties.
- Our results show the presence of impurity atoms reduces the spin filtering properties.

GRAPHICAL ABSTRACT

With the decrease of wall thickness, not only the indirect transition becomes more and more important during the emission process due to the stronger surface band bending effects and even turns into the main emission when the wall thickness decreases to 25 nm, but also the PL intensity is enhanced step by step due to the less defect density and higher carrier concentration caused by the introduction of chlorine in ZNTs during the etching process.

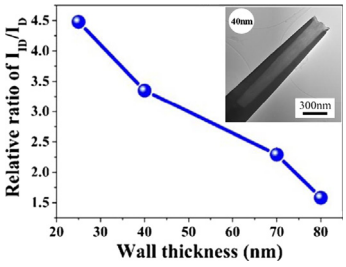

ARTICLE INFO

Article history:
Received 12 May 2013
Accepted 3 June 2013
Available online 14 June 2013

Keywords:
Nanotubes
Wall thickness
Surface band bending
Indirect transition
PL intensity enhancement

ABSTRACT

The ZnO nanotubes (ZNTs) with different wall thickness were fabricated by a simple wet chemical approach. Both indirect and direct transitions contribute to the UV emission of ZNTs. With the decrease of wall thickness, not only the indirect transition becomes more and more important during the emission process due to the stronger surface band bending effects and even turns into the main emission when the wall thickness decreases to 25 nm, but also the PL intensity is enhanced step by step due to the less defect density and higher carrier concentration caused by the introduction of chlorine in ZNTs during the etching process.

1. Introduction

Since the carbon nanotubes had been firstly reported by Iijima in 1991 [1], great interests have been focused on the controllable synthesis and applications of different nanotubes. So far, the carbon, TiO_2, SnO, and ZnO nanotubes have been widely used in the field of solar cell and sensor applications owing to its special hollow structure and larger surface area to fulfill the demand for high efficiency and activity [2–6].

Recently, ZnO nanotubes (ZNTs) as an ionic semiconductor with a wide and direct band gap (3.4 eV) have attracted lots of academic attentions, which have been widely studied on their application in

* Corresponding author at: Institute of Condensed State Physics, Jilin Normal University, Siping 136000, China. Tel.: +86 434 3294566; fax: +86 434 3294566.
E-mail address: jhyang1@jlnu.edu.cn (J. Yang).

1386-9477/$ - see front matter © 2013 Elsevier B.V. All rights reserved.
http://dx.doi.org/10.1016/j.physe.2013.06.003

the fields of dye (quantum dots)-sensitized photovoltaic cells [6,7] and bio/gas sensors [8,9]. So far, the most direct route to prepare ZnO nanotubes is the template-assisted electrochemical deposition method, in which the nanochannels of anodic aluminum oxide membrane are usually used [10]. However, the ordered arrays may be destroyed when the template is removed. Another popular strategy is a solvothermal method, which is performed under high pressure in an autoclave [11–13]. However, in this approach, the control of the size and wall thickness of nanotubes during the growth process remains complex and difficult. Though extensive efforts have been made to fabricate ZNTs, it is still a challenge to realize the large-scale growth of ZNTs with controllable size and dimension [6–9]. Moreover, it is well known that the specific surface area has great influence on the optical properties of nanostructures. Once the wall thickness or tube depth has been tuned, the corresponding change in the optical properties will happen due to the variation of specific surface area. However, so far, the effects of wall thickness/tube depth on the optical properties of ZNTs are rarely reported.

In this paper, we will present a simple wet chemical approach to fabricate the ZNTs with different wall thickness. The effects of wall thickness on the optical properties of ZNTs have been investigated in detail.

2. Experiments

The ZNTs used in this investigation were synthesized by two-step process, i.e. growth of ZnO nanorods (ZNRs) and chemical etching process for converting ZNRs into ZNTs. Firstly, ZNRs were grown on Si substrates by the chemical bath deposition (CBD) method, which also includes a two-steps process, i.e. a substrate treatment prior to the CBD growth. The pre-treatment of the substrates, by coating the substrate for different times with a 5 mM solution of zinc acetate dihydrate ($Zn(OOCCH_3)_2 \cdot 2H_2O$) dissolved in pure ethanol, was used to control the diameter of ZnO nanorods. In the CBD growth, the 0.1 M aqueous solutions of zinc nitrate hexahydrate [$Zn(NO_3)_2 \cdot 6H_2O$, 99.9% purity] and 0.1 M aqueous solutions of methenamine ($C_6H_{12}N_4$, 99.9% purity) were first prepared and mixed together. The pre-treated Si substrates were immersed into the aqueous solution and kept at 93 °C for 3 h with sealing the beaker. Subsequently, a set of ZNRs samples with the diameter of 280 nm were respectively converted into ZNTs by chemical etching process for different time (6 h, 7 h, 9 h, and 10 h). The chemical etching process was carried out by suspending the ZNRs sample upside down in 100 ml aqueous solution of potassium chloride (KCl) with 5 M concentration at 95 °C.

Scanning electron microscopy (SEM) pictures were recorded by using a JEOL JSM-6301F. ZnO nanotubes were scratched off the substrate to analyze their structural properties by transmission electron microscopy (TEM) using a high-resolution microscope of JEM-2100HR from Japan operating at 200 kV. A drop of an ethanol suspension containing the nanotubes was deposited on a copper grid with lacy carbon for TEM observations. Room temperature photoluminescence (PL) measurements were carried out. A CCD detector (Spectrum One) and monochromator HR460 from Jobin Yvon-Spex were used to disperse and detect the ZnO emission. Laser line with a wavelength of 266 nm from a diode laser (Coherent Verdi) pumped resonant frequency doubling unit (MBD 266) was used as excitation source. Time resolved PL (TRPL) was performed by using an excitation laser line from a frequency tripled sapphire: Ti laser emitting at 266 nm, a 0.3 m monochromator and a streak camera. The spectral resolution is about 1 meV and the time resolution is 7 ps. The measurements were done under weak excitation conditions (0.5 W/cm^2). XPS measurements were performed using a Scienta® ESCA200 spectrometer in ultra-high vacuum (UHV) with a base pressure of 10^{-10} mbar. The measurement chamber is equipped with a monochromatic Al (Kα) X-ray source providing photon with $h\upsilon = 1486.6$ eV. The XPS experimental condition was set so that the full width at half maximum (FWHM) of the clean Au $4f_{7/2}$ line was 0.65 eV. All spectra were measured at a photoelectron take-off angle of 0° (normal emission) and room temperature. The binding energies in the XPS spectra were obtained by reference to the Fermi level with an error of ±0.1 eV.

3. Results and discussions

3.1. Structural characterization of ZNTs

The SEM and TEM techniques were used to characterize the morphologies and structures of ZNRs and ZNTs. The SEM images of the as-grown ZNRs with 280 nm diameters and corresponding converted ZNTs with different wall thickness are shown in Fig. 1a–e. The hexagonally shaped nanorods uniformly cover the entire Si (0 0 1) substrate with high density as shown in Fig. 1a. From Fig. 1b–e, we can observe that the wall thickness of ZNTs decreased step by step with prolonging the etching time. The wall thickness can be determined to be 80 nm, 70 nm, 40 nm and 25 nm corresponding to the etching time of 6 h, 7 h, 9 h and 10 h, respectively. The etching mechanism can be described as follows: Elias et al. pointed out that the selective etching to form hollow structures should be related with the initial crystal structure of ZNRs since no assistant reagents existed in the etching solution [14]. Two main factors will determine the conversion process from ZNRs to ZNTs. On one hand, the distinctive ZnO crystal habit exhibits a polar basal (0 0 0 $\bar{1}$)/top (0 0 0 1) planes and six nonpolar (1 0 $\bar{1}$ 0) planes parallel to c-axis. The two polar planes are metastable due to the high surface energy, while the nonpolar (1 0 $\bar{1}$ 0) planes are the most stable ones due to the lower surface energy. So the Cl-ions might be preferentially adsorbed onto the top polar (0 0 0 1) surface of the nanorods, which may result in the formation of a highly water-soluble zinc chloride complex such as $ZnCl^+$, inducing the gradual dissolution of the nanorods core from the tip toward the bottom. As a whole effect, the etching rate is faster along polar plane than nonpolar planes. On the other hand, the defects in the ZNRs preferentially located near the crystal center, so that the preferential etching occurs from the center to form the tubular structures.

The structure of ZNTs is also characterized by TEM, high-resolution TEM (HRTEM) and selected area electron diffraction (SAED) images, as shown in Fig. 1f–h. The TEM image in Fig. 1e shows the hollow structure of one single tube. The HRTEM image in Fig. 1f was taken out at the tube top area in Fig. 1e. It clearly reveals a lattice spacing of 0.52 nm which corresponds to the distance of the (0 0 1) crystal plane of wurtzite ZnO (hexagonal structure with cell constants of $a = 3.249$ Å and $c = 5.206$ Å). The SAED pattern in Fig. 1g indicates that the ZnO nanotube is single crystal with wurtzite structure.

3.2. Optical properties of ZNTs

The room temperature PL spectra of ZNRs and ZNTs with different wall thickness are illustrated in Fig. 2(a). All the samples show a dominant UV emission and a weak deep level emission (DLE) centered at ~520 nm. The UV emission band is related to a near band-edge transition of ZnO, namely, the recombination of the free excitons. The DLE band had recently been identified and at least two intrinsic defect origins (V_O and V_{Zn}) with different optical characteristics were claimed to contribute to this DLE band [15–17]. It is interesting to notice that the UV emission of ZNTs exhibit an

asymmetric spectrum with an obvious left shoulder, as clearly shown in the inset of Fig. 2(a). In our previous report, we pointed out that both direct (D) and indirect (ID) transitions contribute to the UV emission due to the surface band bending effects in the ZNTs [18]. While, for ZNRs sample, the UV emission is mainly originated from the D transition. To reveal the dependence of D and ID transition on the wall thickness of ZNTs, all the UV emission spectra have been fitted by the Gaussian functions, as shown in Fig. 2(b). We can see

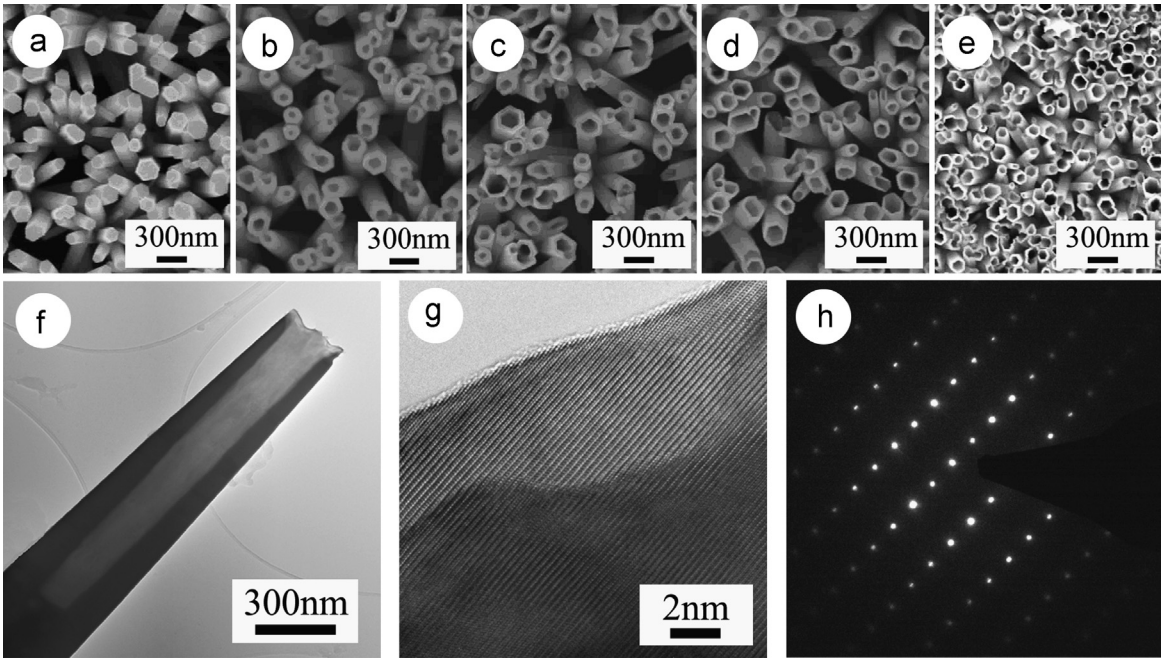

Fig. 1. SEM images of ZNRs (a) and ZNTs for etching different time (b) 6 h, (c) 7 h, (d) 9 h and (e)10 h; TEM (f), HRTEM (g) and SAED (h) images of ZNTs for etching 9 h.

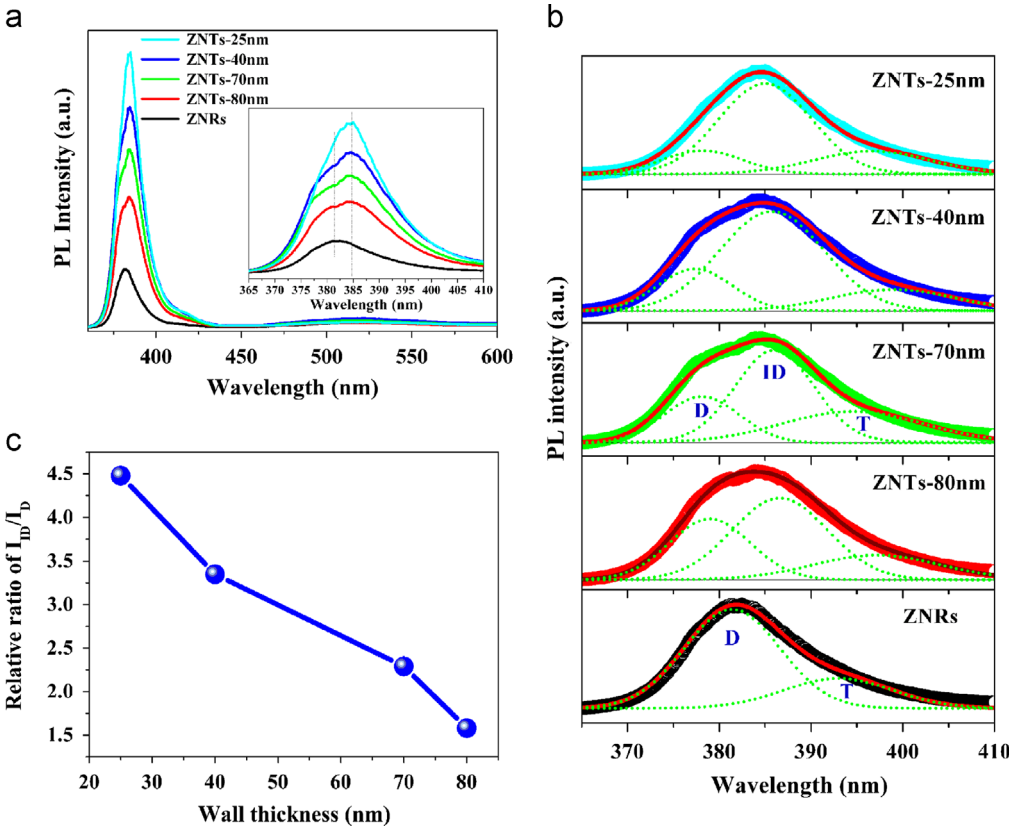

Fig. 2. (a) Room temperature PL spectra of ZNRs and ZNTs with different wall thickness, the inset is the large magnification image in the UV region; (b) Fitting results of UV emission. A good fitting could be obtained when deconvolutions of two Gaussian peaks corresponding to the direct transition (D) and PL tail (T) are used for the spectrum of ZNRs, while three Gaussian peaks of D, indirect transition (ID) and T are needed to get a good fitting for all the spectra of ZNTs; (c) Relative intensity ratio of indirect transition to direct transition (I_{ID}/I_D) via wall thickness of ZNTs.

that all the PL spectra contain a low-energy tail (T) emission, which is associated to the phonon replica of free exciton or localized excitons [19,20]. A good fitting could be obtained when deconvolutions of two Gaussian peaks corresponding to the D and T are used for the spectrum of ZNRs, while three Gaussian peaks of D, ID and T are needed to get a good fitting for all the spectra of ZNTs. The dependence of relative intensity ratio of indirect transition to direct transition (I_{ID}/I_D) on the wall thickness of ZNTs has been summarized in the Fig. 2(c). Clearly, with the decrease of wall thickness in ZNTs, the contribution of ID transition in UV emission process becomes more and more important due to the increasing specific surface area.

Moreover, usually, the existence of indirect radiative recombination will strongly suppress the emission intensity due to reduced electron-hole wave function overlapping. However, in our case, the PL intensity of ZNTs is much higher than that of ZNRs as a whole. Furthermore, the PL intensity of ZNTs enhances step by step with the decrease of their wall thickness, which disobeys the normal opinion about the variation tendency, since not only the contribution of ID transition becomes more and more important, but the mass of ZnO decreases step by step as well. We further performed the measurement of low temperature PL and TRPL spectra. As shown in the Fig. 3(a), clearly, the integral PL intensity follows the same variation tendency with decreasing the wall thickness of ZNTs. For the TRPL spectrum obtained from ZNTs in Fig. 3(b), the decay exhibits a single exponential curve, which apparently indicates that no surface recombination exists in the ZNTs [21–24]. According to the fitting results, the decay time (τ) is 10 ps, 24 ps, and 34 ps corresponding to the ZNTs with 80 nm, 40 nm and 25 nm wall thickness, respectively. This variation tendency has a good agreement with the results of room and low temperature PL, which further proves the facticity of room temperature PL results.

The UV emission process consists of radiative and non-radiative recombinations. Generally, the PL decay rate of a semiconductor includes two components, i.e. radiative and non-radiative decay rates with a relationship of $\tau^{-1} = \tau_{NR}^{-1} + \tau_R^{-1}$, where τ, τ_{NR} and τ_R is the time constant of PL, non-radiative and radiative decay, respectively [25]. The measured effective PL decay τ will strongly depend on the relative value of non-radiative τ_{NR} and radiative time τ_R. Apparently, the value of τ in our case is so much shorter compared to other reports on the ZnO nanorods (70 ps for the one grown with the same method [26]). Therefore, we can incipiently conclude that the non-radiative recombination process dominates the life time in our case. Usually, the effective non-radiative recombination mainly originates from the capture of excitons and carriers by deep centers at defects and/or impurities. Therefore, it is necessary to analyze the defects in the ZNRs and ZNTs. The micro-Raman and resonant Raman scattering (RRS) measurement has been used to monitor the change of defects in the chemically grown ZNRs [22]. Fig. 4

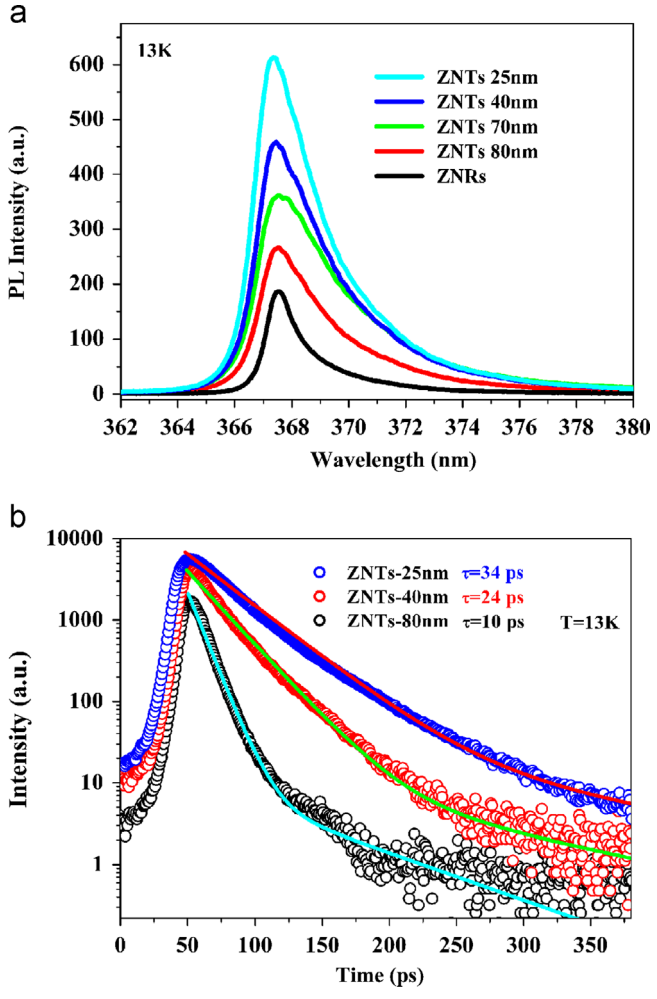

Fig. 3. (a) Low temperature PL spectra of ZNRs and ZNTs with different wall thickness (13 K); (b) Time-resolved PL (TPRL) spectra of ZNTs with 80 nm, 40 nm and 25 nm wall thickness obtained at 13 K. The color empty circle and solid lines presents the experimental data and fitting results, respectively. (For interpretation of the references to color in this figure legend, the reader is referred to the web version of this article.)

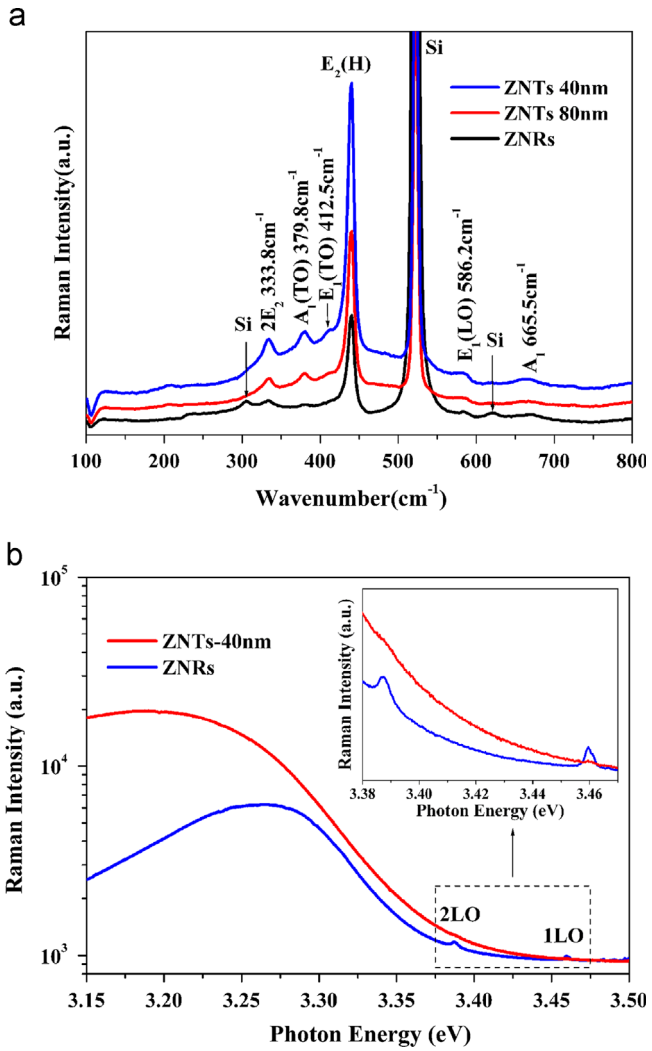

Fig. 4. (a) Micro-Raman spectra of ZNRs and ZNTs with 488 nm excitation; (b) Room temperature emission spectra of ZNRs and ZNTs with 351.1 nm excitation.

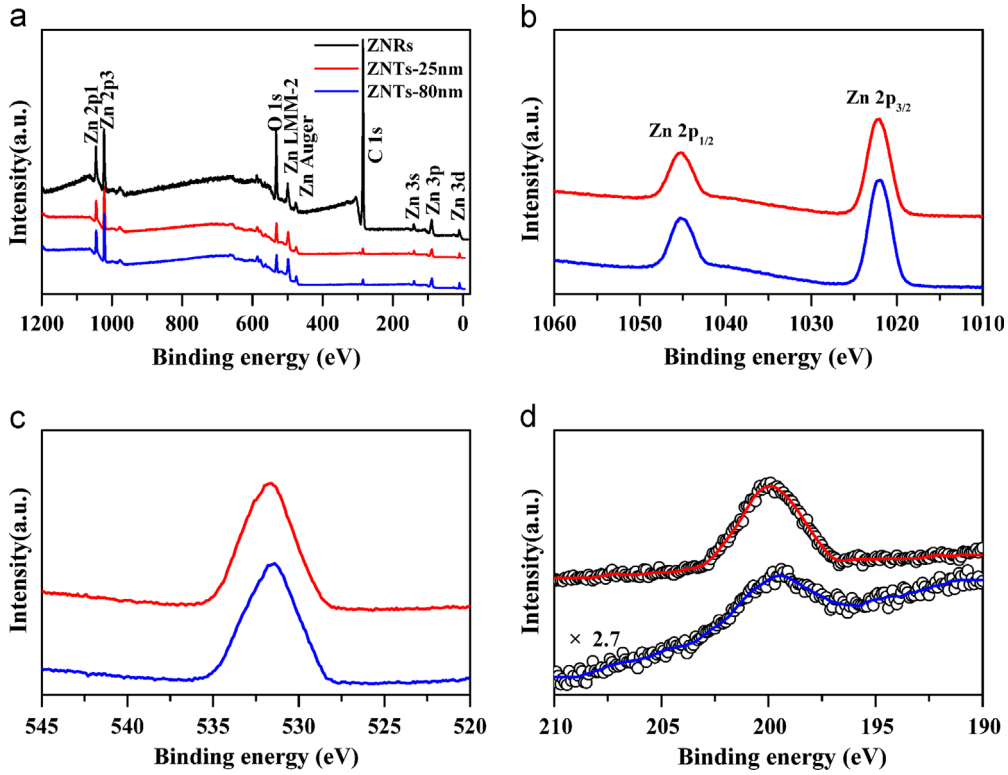

Fig. 5. (a) XPS survey spectra of ZNRs and ZNTs with 80 nm and 25 nm wall thickness, where the labels indicate the origins of the corresponding peaks; (b) Zn 2p (c) O 1 s and (d) Cl 2p XPS spectra of ZNTs with 80 nm and 25 nm wall thickness.

(a) illustrates the room temperature micro-Raman spectra of ZNRs and ZNTs with 488 nm excitation. The peaks at 333.8 cm^{-1}, 379.8 cm^{-1}, 412.5 cm^{-1}, 439.2 cm^{-1}, 586.2 cm^{-1}, and 665.5 cm^{-1} can be ascribed to the $2E_2$, A_1(TO), E_1(TO), E_2, E_1(LO) and A_1 mode, respectively, which indicates both ZNRs and ZNTs own the typical wurtzite structures [27]. Moreover, with decreasing the wall thickness, the Raman scattering intensity enhances step by step, implying that the crystal quality of ZNTs turns better and better, i.e. less defects in ZNTs. Moreover, Fig. 4(b) illustrates the emission spectra of ZNRs and ZNTs with 351.1 nm excitation. The spectrum from ZNRs consists of an RRS progression based on a fundamental 1LO band at 3.459 eV and its multiple-LO scatterings. Since the Raman scattering is performed with backscattering geometry, the main contribution to the RRS signal comes from the A_1-LO mode [22]. The A_1-LO mode reflects the defect density in the ZNRs, that is, the RRS lines intensity will be stronger if there are more defects in the sample. We can see in Fig. 4(b) that no RRS lines appear in the spectrum of ZNTs. To see it clearly, the region marked by the black dot box has been enlarged and shown in the inset. In contrast, the strong Raman peaks of 1LO and 2LO (A_1-LO mode) appear in the spectrum of ZNRs, further indicating more defects in them.

To thoroughly reveal the origination of PL intensity enhancement of ZNTs, we performed the XPS measurement on the ZNRs and ZNTs with 80 nm and 25 nm wall thickness to identify their chemical compositions, by which maybe we can find the reason of defect reduction in ZNTs. The survey XPS spectra of ZNRs and ZNTs are presented in Fig. 5(a), in which all of the peaks can be only ascribed to Zn, O, and C elements as labeled in the image. Here we would like to point out that, for all the XPS spectra, the binding energies have been calibrated by taking the carbon C1s peak (285.0 eV) as reference. The Zn 2p and O 1s XPS spectra in Fig. 5(b) and (c) have not shown big difference for ZNTs with 80 nm and 25 nm wall thickness. But it is worth to note that the relative intensity of C1s signal is extremely strong for ZNRs in comparison with that of ZNTs. Since the vacuum level of equipment kept same during the measurement for all the samples, such big difference in intensity only can be attributed to the native chemical composition of the samples. For ZNRs, the surface will be attached by lots of chemical group of $–CO_3$ due to the large amount of them in the growth solution of $Zn(NO_3)_2$ and $C_6H_{12}N_4$. While, during the etching process of ZNTs, we can imagine that the $–CO_3$ group will be released and further substituted by the chlorine (Cl) ions. In order to verify this, XPS technique was used to detect the Cl signal from the ZNTs. As shown in Fig. 5(d), we can obviously obverse the signal of Cl element in both ZNTs samples with different wall thickness. Moreover, the intensity of Cl 2p signal is enhanced with decreasing the wall thickness of ZNTs. It is mainly caused by the enlarged specific surface area, which provides more available sites for the chlorine ions. Cui et al. reported in their work that the introduction of Cl can reduce the density of oxygen vacancies in ZnO nanowires since Cl is apt to substitute oxygen in ZnO [28]. Thus, the existence of large amount of Cl element in the ZNTs is the main reason for their better crystal quality in comparison with ZNRs. In addition, Chikoidze et al. suggested that the use of non-metallic dopants in substitution to oxygen was a better way to achieve higher carrier concentration and mobility while keeping good transparency of ZnO [29]. Lee et al. confirmed experimentally that the carrier concentration would increase with Cl doping in ZnO film [30]. Plus, the carriers originated from Cl can be transported to the ZnO very fast due to their close contact, so that the PL intensity will be further enhanced. Thus, with the decrease of wall thickness in ZNTs, the enhanced PL intensity step by step can be attributed to the less defect density and higher carrier concentration caused by the introduction of Cl in ZNTs during the etching process.

4. Conclusions

In this work, we successfully reveal the effects of wall thickness of ZNTs on their optical properties. The results show that not only the wavelength but also the intensity of UV emission can be

modulated by the wall thickness of ZNTs. In comparison with ZNRs, the ZNTs with 25 nm wall thickness exhibits an excellent UV emission, which can be prospected to be a promising candidate for UV sensor and detector. In addition, the reveal of Cl contribution to the UV emission of ZNTs will stimulate more theoretical and experimental investigations about Cl-doped ZnO nanostructures in the future.

Acknowledgments

The authors would like to acknowledge financial support for this work from the National Nature Science Foundation of China (Grant nos. 11204104, 61178074 and 61008051), Program for the Development of Science and Technology of Jilin province (Item nos. 20110415, 201115219 and 20100113), program for the Master Students' Scientific and Innovative Research of Jilin Normal University (Item nos. 201112, 201101 and 201139).

References

[1] S. Iijima, Nature 354 (1991) 56.
[2] K. Shankar, G.K. Mor, H.E. Prakasam, S. Yoriya, M. Paulose, O.K. Varghese, C.A. Grimes, Nanotechnology 18 (2007) 065707.
[3] P. Roy, S. Berger, P. Schmuki, Angewandte Chemie International Edition 50 (2011) 2904.
[4] X. Chen, Z. Guo, W.H. Xu, H.B. Yao, M.Q. Li, J.H. Liu, X.J. Huang, S.H. Yu, Advanced Functional Materials 21 (2011) 2056.
[5] J. Ye, H. Zhang, R. Yang, X. Li, L. Qi, Small 6 (2) (2010) 296.
[6] A.B.F. Martinson, J.W. Elam, J.T. Hupp, M.J. Pellin, Nano Letters 7 (2007) 2183.
[7] Q.F. Zhang, C.S. Dandeneau, X.Y. Zhou, G.Z. Cao, Advanced Materials 21 (2009) 4087.
[8] K. Yang, G.W. She, H. Wang, X.M. Ou, X.H. Zhang, C.S. Lee, S.T. Lee, Journal of Physical Chemistry C 113 (2009) 20169.
[9] Z.H. Jing, J.H. Zhan, Advanced Materials 20 (2008) 4547.
[10] L. Li, S.S. Pan, X.C. Dou, Y.G. Zhu, X.H. Huang, Y.W. Yang, G.H. Li, L.D. Zhang, Journal of Physical Chemistry C 111 (2007) 7288.
[11] L. Vayssieres, K. Keis, A. Hagfeldt, S.E. Lindquist, Chemistry of Materials 13 (2001) 4395.
[12] S. Kar, S. Santra, Journal of Physical Chemistry C 112 (2008) 8144.
[13] J.X. Wang, X.W. Sun, H. Huang, Y.C. Lee, O.K. Tan, M.B. Yu, G.Q. Lo, D.L. Kwong, Applied Physics A 88 (2007) 611.
[14] J. Elias, Ramon Tena-Zaera, G.Y. Wang, C. Le´vy-Cle´ment, Chemistry of Materials 20 (2008) 6633.
[15] Q.X. Zhao, P. Klason, M. Willander, H.M. Zhong, W. Lu, J.H. Yang, Applied Physics Letters 87 (2005) 211912.
[16] T.M. Børseth, B.G. Svensson, A.Y. Kuznetsov, P. Klason, Q.X. Zhao, M. Willander, Applied Physics Letters 89 (2006) 262112.
[17] P. Klason, T.M. Børseth, Q.X. Zhao, et al., Solid State Communication 145 (2008) 321.
[18] L.L Yang, Q.X Zhao, M.Q Israr, J.R. Sadaf, M. Willander, G. Pozina, J.H. Yang, Journal of Applied Physics 108 (2010) 103513.
[19] J.W. Sun, Y.M. Lu, Y.C. Liu, D.Z. Shen, Z.Z. Zhang, B. Yao, B.H. Li, J.Y. Zhang, D.X. Zhao, X.W. Fan, Journal of Applied Physics 102 (2007) 043522.
[20] J. Jie, G. Wang, Y. Chen, X. Han, Q. Wang, B. Xu, J.G. Hou, Applied Physics Letters 86 (2005) 031909.
[21] Q.X. Zhao, L.L. Yang, M. Willander, B.E. Sernelius, P.O. Holtz, Journal of Applied Physics 104 (2008) 073526.
[22] L.L. Yang, Q.X. Zhao, M. Willander, J.H. Yang, I. Ivanov, Journal of Applied Physics 105 (2009) 053503.
[23] L.L. Yang, Q.X. Zhao, M. Willander, X.J. Liu, M. Fahlman, J.H. Yang, Applied Surface Science 256 (2010) 3592.
[24] L.L. Yang, Q.X. Zhao, M. Willander, X.J. Liu, M. Fahlman, J.H. Yang, Crystal Growth and Design 10 (2010) 1904.
[25] J.Y. Shi, J. Chen, Z.C. Feng, T. Chen, X.L. Wang, P.L. Ying, C. Li, Journal of Physical Chemistry B 110 (2006) 25612.
[26] C. Bekeny, T. Voss, B. Hilker, J. Gutowski, R. Hauschild, H. Kalt, B. Postels, A. Bakin, A. Waag, Journal of Applied Physics 102 (2007) 044908.
[27] T.C. Damen, S.P.S. Porto, B. Tell, Physical Review 142 (2001) 570.
[28] J.B. Cui, Y.C. Soo, T.P. Chen, U.J. Gibson, Journal of Physical Chemistry C 112 (2008) 4475.
[29] E. Chikoidze, M. Modreanu, V. Sallet, O. Gorochov, P. Galtier, Physica Status Solidi (A) 205 (2008) 1575.
[30] J. Lee, E. Park, N.G. Subramaniam, J. Lee, J. Lee, J. Lee, T. Kang, Current Applied Physics (2012), http://dx.doi.org/10.1016/j.cap.2012.05.019.